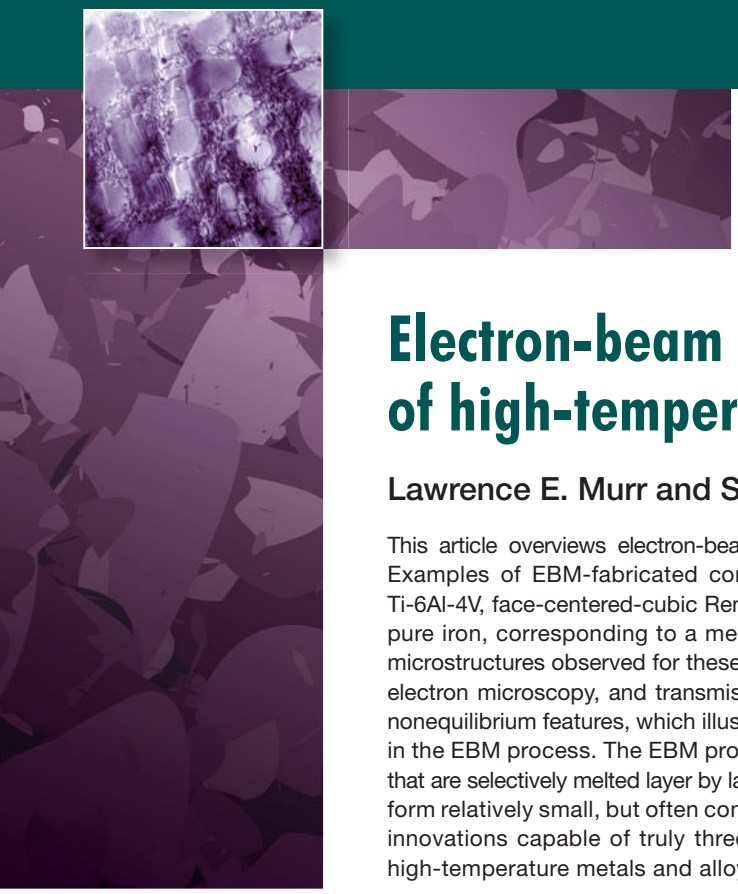


Electron-beam additive manufacturing of high-temperature metals

Lawrence E. Murr and Shujun Li

This article overviews electron-beam melting (EBM), including process optimization issues. Examples of EBM-fabricated components described include hexagonal close-packed Ti-6Al-4V, face-centered-cubic René 142 (a Ni-based superalloy), and body-centered-cubic pure iron, corresponding to a melt temperature range from 1375°C to 1630°C. Residual microstructures observed for these fabricated components by optical microscopy, scanning electron microscopy, and transmission electron microscopy include equilibrium as well as nonequilibrium features, which illustrate prospects for novel structure–property manipulation in the EBM process. The EBM process relies on available pre-alloyed, precursor powders that are selectively melted layer by layer by a computer-aided design scanned electron beam to form relatively small, but often complex, products or components. Direct metal deposition innovations capable of truly three-dimensional metal printing are described, especially high-temperature metals and alloys for future additive manufacturing technologies.

Introduction

Electron-beam melting (EBM) has recently become one of the standard additive manufacturing technologies for metals. Commercial EBM systems are available to a limited extent, currently dominated by Arcam AB, Sweden. The Arcam EBM system, illustrated schematically in **Figure 1**, relies on gravity feed of an optimized metal (or alloy) powder (Figure 1 inset), usually prepared by rapid solidification processing. Powders in cassettes flow by gravity onto a raked bed where the electron beam is selectively scanned using computer-aided design (CAD) software to heat and melt each raked layer; these usually consist of roughly three powder particle diameters in thickness. As each raked layer is selectively melted, the build platform drops down by a layer thickness (usually 50–100 μm) and a new powder bed is formed; the process is then repeated.

In the Arcam system, the build volume (in vacuum) is limited to about 0.03 m^3, which allows only small product fabrication. In addition, many high-temperature metal products require pre-alloyed powders, and fabricated products requiring intricate internal structures must be designed to allow the unmelted powder to be conveniently removed. Consequently, closed cellular structures cannot be fabricated since unmelted powder remains within the closed cells.

In this article, we examine the fundamental aspects of additive EBM fabrication, including process optimization and limitations. Selective examples of EBM processing of high-temperature metals and alloys include (with their melting points in parentheses) Ti-6Al-4V (1630°C), the Ni-based superalloy René 142 (1375°C), and Fe (1537°C). These metals represent hexagonal close-packed (hcp), face-centered-cubic (fcc), and body-centered-cubic (bcc) crystal structures, respectively. These metals are used in a range of products and applications, including aerospace components (Fe, Ti-6Al-4V and Ni-based superalloys), orthopedic appliances (Ti-6Al-4V), turbine system components (René 142), and special property components such as magnetic materials (Fe).

Fundamental issues in contemporary EBM: Process control and optimization

The melt (L)–solidification (S) process characteristics of powder bed-layer additive manufacturing by EBM are shown in **Figure 2**. The local temperature in the layer thickness (t) can be represented generally by:

$$T = Q\,(1-R)/\rho\,C_p t, \qquad (1)$$

where Q is the power density, R is the electron reflectivity, C_p is the heat of fusion, and ρ is the powder bed density, which increases with melting of the scanned layer. It can be envisioned that EBM process optimization will involve the beam scan

Lawrence E. Murr, Department of Metallurgical, Materials and Biomedical Engineering, The University of Texas at El Paso, USA; lemurr@utep.edu
Shujun Li, Institute of Metal Research, Chinese Academy of Sciences, China; shjli@imr.ac.cn
doi:10.1557/mrs.2016.210

© 2016 Materials Research Society
https://doi.org/10.1557/mrs.2016.210 Published online by Cambridge University Press

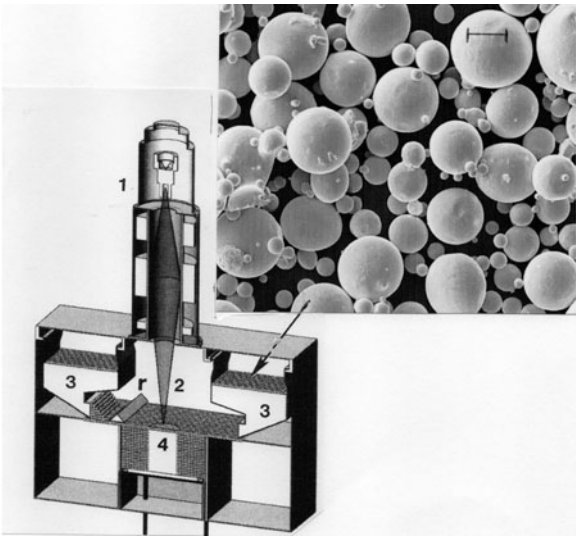


Figure 1. Schematic view of Arcam electron-beam melting (EBM) system. The inset shows a scanning electron microscope (SEM) image of Inconel 625 (Ni-based superalloy) powder typical of precursor powders for EBM. (1) The electron gun (60 kV) and electron optical system; (2) the scanning electron beam; (3) powder cassettes; (4) the build product table. Note: r, powder rake. Magnification marker in the SEM image is 40 μm.

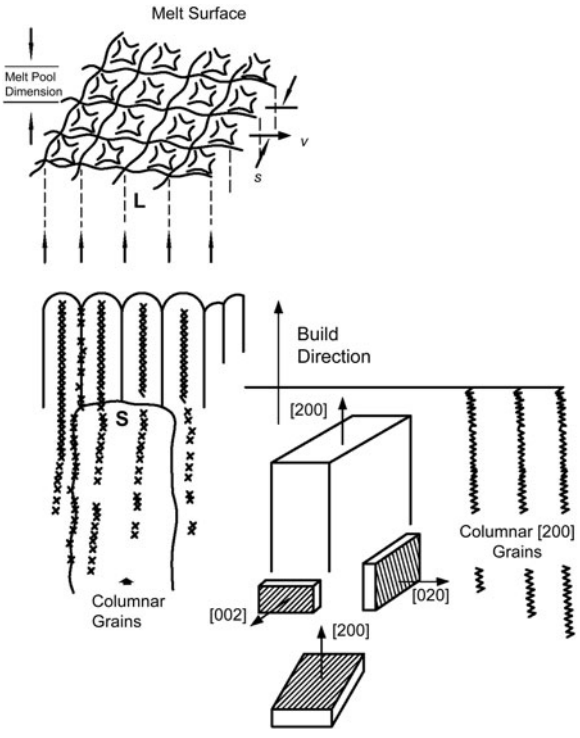


Figure 2. Schematic rendering of melt (L)–solidification (S) growth in electron-beam melting, which can promote columnar (directional) microstructures. Preferred crystal orientations for face-centered-cubic metals and alloys are also shown. Note: *v*, scan speed; *s*, scan lines.

speed (v), the power density (Q), and the beam focus (beam radius, r), where:

$$Q = \frac{\text{power absorbed}}{2\pi r^2 t}, \quad (2)$$

as well as the scan strategy (speed, direction, size, and current of the electron beam),[1] including preheating of the powder bed and variations in the melt scan or scan direction (x, y). Scan-strategy variations will correspondingly influence the distance between scan lines (s in Figure 2) or their overlap.

When the beam is scanned in the x- and y-directions (in the plane perpendicular to the build [z] direction), a melt pool develops with the corresponding scan dimension (s in Figure 2) and, with repeated melt-solidification events in successive powder layers, columnar microstructures can develop, as illustrated schematically in Figure 2. As a result of the localized thermokinetics within the melt pool (Figure 2), novel microstructures can develop within columnar grains to form unique architectures. The lower right image in Figure 2 also shows that columnar grains can adopt preferred orientations, often characteristic of minimum energy directions corresponding to specific crystal unit cells: [002] for fcc and [110] for bcc. However, there are often subtle variances in the beam scan (e.g., speed, spacing) and impurities in the powder layer that will interrupt the columnar, preferred crystallographic growth. For hcp crystal structures, preferred orientations are less common than more equiaxed or truncated microstructures.

Powder purity, morphology, and particle-size distribution are important issues in optimizing the EBM process. The scanning electron microscope image in Figure 1 shows a typical example of a high-temperature metal powder (in this case, the Ni-based superalloy Inconel 625). Preferred powder particles are spherical and their size distribution (as shown in Figure 1) allows effective filling of interstitial volumes in the raked powder bed. This process is also characterized by the particle flowability. In addition, impurities and impurity particles in the powder create beam tripping (where the beam is instantaneously interrupted), often resulting in poorly melted regions, while excess water vapor or oxidation of powders can hinder the melt formation.

In some cases, prebaking of the powders in vacuum and transfer under inert atmospheres can improve the powder melt efficiency. Preheating the powder layers by beam scanning prior to the melt scan is also a crucial step in assuring efficient melting. Gaytan et al.[2] explored many issues relating to beam power, scan speed, and other build parameters, including melt efficiency and the reuse of powders such as Ti-6Al-4V. They described a quality control concept to examine and certify products nondestructively. Gong et al.,[3] Smith et al.,[4] Korner,[5] and several other recent review articles summarize many of these features and manufacturing advances by EBM over the past decade.

Examples of high-temperature metals fabricated by EBM

Ti-6Al-4V

Ti-6Al-4V is perhaps the most widely EBM-fabricated high-temperature metal because of its applications in aerospace

https://doi.org/10.1557/mrs.2016.210 Published online by Cambridge University Press

components and a variety of biomedical components that require quick and adjustable design.[2–7] This hcp alloy is essentially a two-phase (α [hcp] + β [bcc]) system that nominally appears as a lenticular α grain structure with β regions in the α grain interfaces as shown in **Figure 3**a. This structure is temperature (or cooling rate) sensitive, and for product fabrication involving small volumes or thin sections that cool rapidly, α becomes thinner and begins to transform to α′ as implied in Figure 3b. α′ dominates in open cellular structures such as mesh and foam geometries.[6] These structures are precursors to the development of a variety of orthopedic implants[6] as well as other components with complex internal structures, such as heat exchangers, where the EBM fabrication strategy allows for convenient removal of internal unmelted powder.

It can be noted on comparing Figure 3a–b that obvious microstructure refinement, which can occur as a reduction in the spacing between α and α′ platelets (from 8 μm to 1 μm [Figure 3a–b]). This results in an increase in microindentation hardness by more than 40%. Corresponding increases in yield strength are also accompanied by a decrease in elongation.

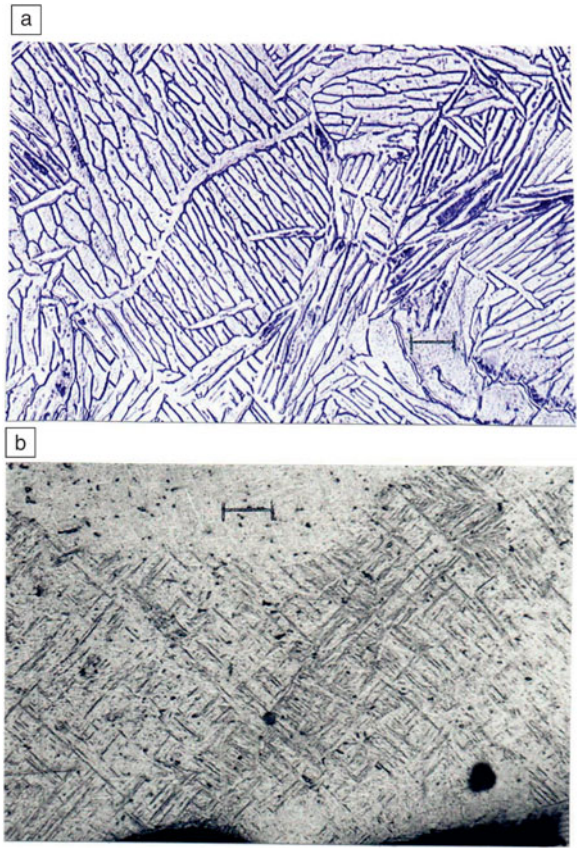


Figure 3. Optical microscope views of electron-beam melting fabricated Ti-6Al-4V components. (a) Double-melt scan to produce large, lens-like α grains (hexagonal close-packed) surrounded by a thin (dark) β (body-centered-cubic) phase. (b) Rapidly cooled thin component section producing closely spaced α′ platelets (dark). Magnification markers are 25 μm.

René 142 Ni-based superalloy

In the development of commercial Ni-based superalloys for directionally grown (cast) turbine blades, cuboidal γ′ (Ni_3 (Al, Ta)) precipitates have played a crucial role.[5] In these alloys, cuboidal Ni_3 (Al, Ta) fcc γ′ precipitates fill the directionally grown blade, and their cuboidal geometry and size relative to their spacing in the fcc Ni-Cr matrix can be engineered (through various heat treatments) to control deformation, especially creep deformation, which begins in the fcc Ni-Cr matrix and then propagates into the Ni_3 (Al, Ta) cuboidal precipitates.

Figure 4 shows a low-magnification, three-dimensional (3D) section view of a Rene 142 Ni-based superalloy (12Co, 6.8Cr, 6.35Ta, C.15Al, 4.9W, 2.8Re, 1.5Mo, 1.5Hf, balance Ni) powder-EBM-fabricated product containing columnar grains growing in the build direction (B). In contrast to the random powder orientations, the vertical and horizontal (plane) sections are strongly (200) and (220) oriented corresponding to Figure 2. Magnified views of 3D sections within the oriented (columnar) grains show the cuboidal γ′ precipitates (Figure 4 inset). As discussed by Oblak and Kear,[8] a higher magnification view in the transmission electron microscope (TEM) (**Figure 5**) illustrates the unique coherent {100} interfaces separating the γ′ cuboids from the fcc Ni-Cr matrix, where a high density of dislocations accommodate some of the coherent interface strain.

It is interesting to note[9] that EBM-fabricated René 142 components contain essentially optimized γ′ cuboidal size as well as the fcc Ni-Cr (γ) matrix thickness separating the γ′ cuboids. This additive manufacturing process, involving a standard layer

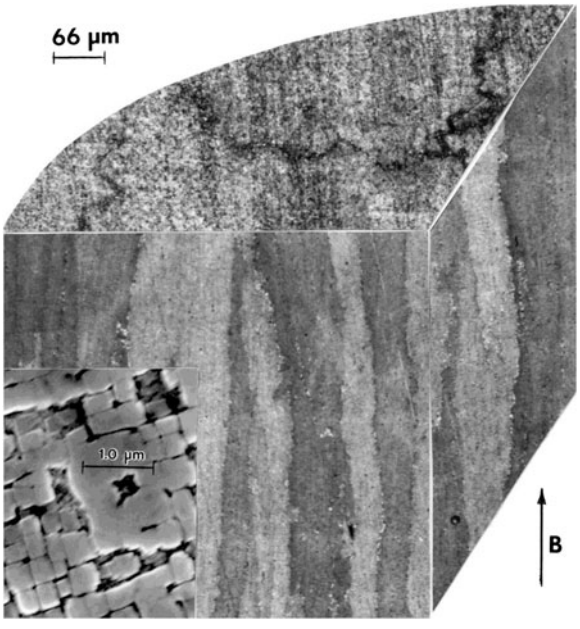


Figure 4. 3D sectional view of a René 142 Ni-based superalloy component exhibiting columnar ⟨200⟩ grains containing cuboidal γ′ phase (face-centered-cubic [fcc]) Ni_3 (Al, Ta) precipitates shown in the scanning electron microscope image inset. Precipitates are separated by fcc Ni-Cr (γ phase). Note: B, build direction (the *z*-direction in Figure 2).[8]

https://doi.org/10.1557/mrs.2016.210 Published online by Cambridge University Press

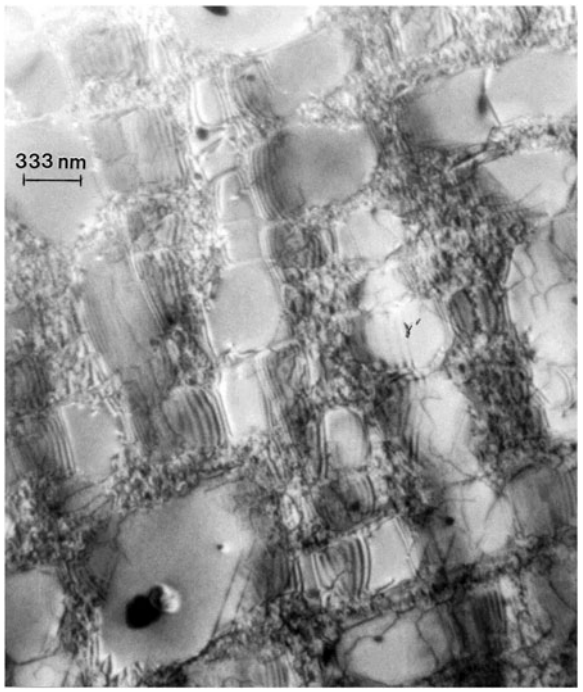


Figure 5. Transmission electron microscope image showing coherent γ/γ′ cuboidal precipitates in René 142 alloy components shown in the scanning electron microscope inset in Figure 4.[8]

preheat scan sequence and the melt scan sequence, fortuitously skips complex annealing schedules normally employed in developing optimized, commercial René 142 turbine blades.

Iron

While Figures 4 and 5 illustrate an example of an fcc, high-temperature superalloy fabricated by EBM, **Figure 6** shows a 3D section view of bcc iron fabricated by EBM. The relatively equiaxed ferrite grain structure shows unusual δ iron precipitates within the bcc (α, ferrite) grains. This nonequilibrium high-temperature (quenched) phase is retained from the rapidly solidified, atomized ferrite-iron powder (Fe, 99.9%, 0.05%°C).[10] The ferrite grains are strongly textured with platelets in the [110] direction, as seen in the x-ray diffraction spectra in **Figure 7**.

The bcc δ phase occurs as thin, irregular platelets coincident with the ferrite {110} and {100} planes. **Figure 8** shows a TEM image of a (111) plane where the δ phase is coincident with the $[1\bar{1}0]$ and $[\bar{1}01]$ directions shown by A and B, respectively. Extended screw dislocations are also prominently featured in the microstructure in Figure 8. For more details about EBM microstructure in solid iron and open cellular structures, see Reference 10.

Summary

We have presented a short review of the EBM process along with a few examples of high-temperature metals fabricated by EBM. The fabrication of Ti-6Al-4V is characterized by

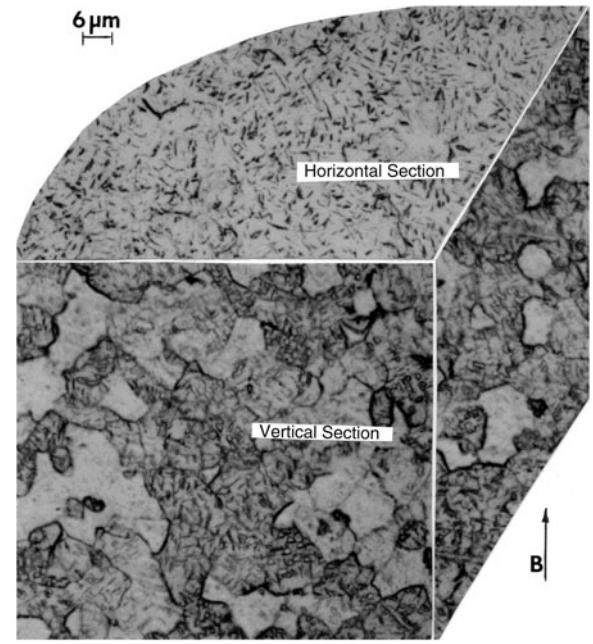


Figure 6. Equiaxed ferrite (body-centered-cubic [bcc]) grains in a pure iron electron-beam melting component containing δ-phase (bcc) nonequilibrium phase platelets. Note: B, build direction.[10]

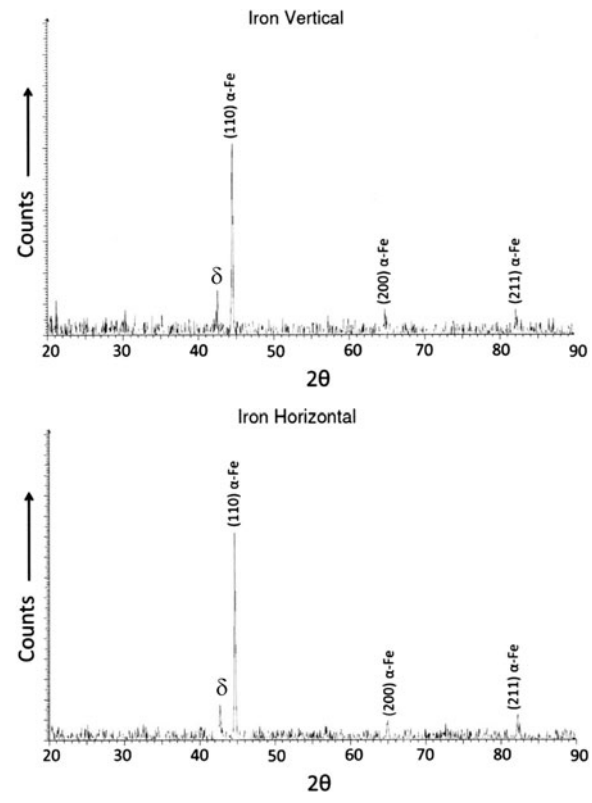


Figure 7. X-ray diffraction spectra corresponding to Figure 6 showing prominent α and δ peaks in vertical and horizontal plane sections.[10]

https://doi.org/10.1557/mrs.2016.210 Published online by Cambridge University Press

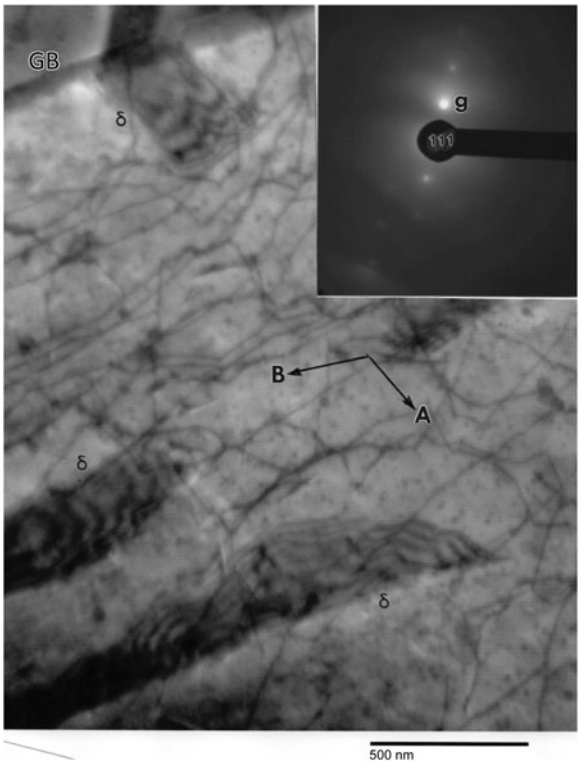


Figure 8. Transmission electron microscope image of a ferrite (111) grain showing irregular δ-phase platelets coincident with the A [1$\bar{1}$0] and B [$\bar{1}$01] directions. The operating reflection is shown at **g**. Note: GB, grain boundary.[10]

microstructures already well known metallurgically: α + β; α + β + α′. In the case of René 142, a Ni-based superalloy characterized by columnar grains with low-angle boundaries, γ′ Ni_3 (Al, Ta) cuboidal precipitates, well known metallurgically since the 1960s, are dominant. In addition, EBM processing produces optimized cube dimensions of 275 nm, spaced by 50 nm in the fcc matrix. In EBM-fabricated iron, however, anomalous δ iron platelets are observed, a microstructure rarely observed in more conventional, equilibrium iron processing.

While EBM fabrication has become an attractive additive manufacturing process for small, high-temperature metal products, including complex geometries and even one-of-a-kind (customized) products, it remains constricted by precursor powder costs (up to 10× solid metal cost) and processing. The inability to fabricate complex, closed-cell structures where unmelted powder cannot be removed also remains a process limitation.

Since the 1990s, there have been a number of investigations aimed at creating metal microdroplets that can be selectively deposited using CAD software to fabricate products by a true 3D printing process.[11–15] **Figure 9** illustrates this concept schematically. Until now, high-temperature metals have evaded such processing, but innovations in direct metal printing head development may someday allow multiple metal deposition from large gantry designs in inert gas or vacuum environments, with

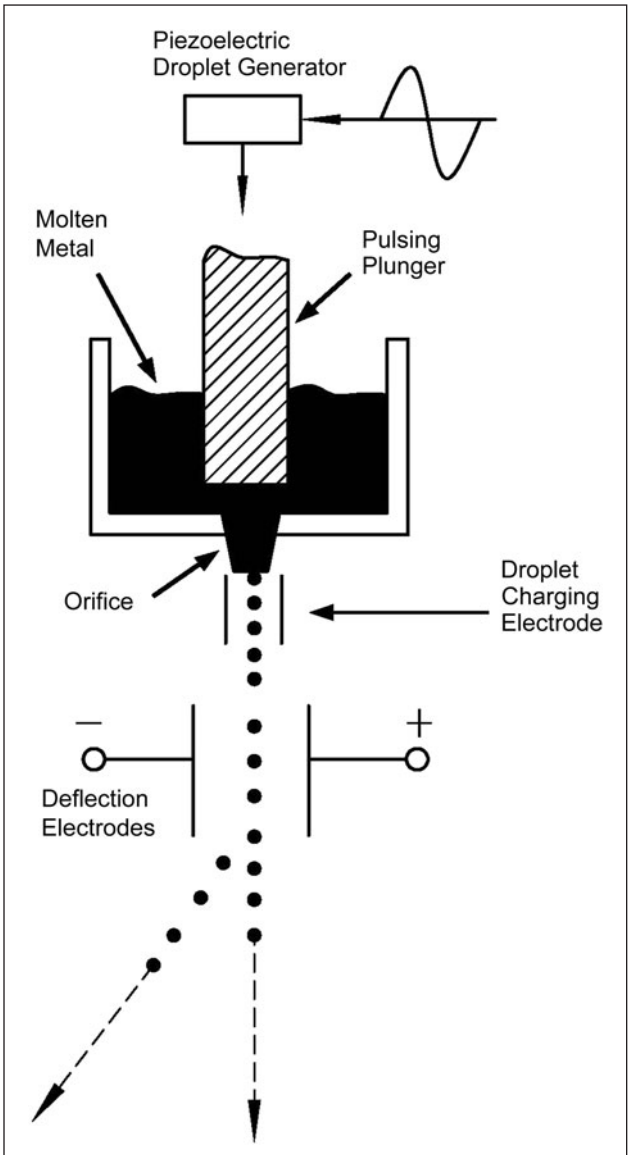


Figure 9. Schematic diagram representing direct metal droplet deposition described conceptually by Orme and Smith. Reprinted with permission from Reference 12. © 2000 The American Society of Mechanical Engineers.

the capability to print large structures and components using auxiliary electron and laser beams for pre- and postprocessing.

Acknowledgments

This research was supported in part by The University of Texas at El Paso, Office of Research and Sponsored Projects, and the National Basic Research Program of China (2012CB933901) and the National Natural Science Foundation of China (51271182).

References

1. S. Bontha, N.W. Klingbeil, P.A. Kobryn, *Mater. Sci. Eng. A* **513–514**, 311 (2009).
2. S.M. Gaytan, L.E. Murr, F. Medina, E. Martinez, M.I. Lopez, R.B. Wicker, *Mater. Technol.* **24** (3), 180 (2009).
3. X. Gong, T. Anderson, K. Chan, *Manuf. Rev.* **1**, 2 (2014).
4. C.J. Smith, F. Derguti, E. Hernandez Nava, M. Thomas, S. Tammas-Williams, S. Gulizia, D. Fraser, I. Todd, *J. Mater. Process. Technol.* **229**, 128 (2015).

https://doi.org/10.1557/mrs.2016.210 Published online by Cambridge University Press

5. C. Korner, *Int. Mater. Rev.* **61** (5), 361 (2016).
6. L.E. Murr, S.M. Gaytan, F. Medina, H. Lopez, E. Martinez, B.I. Machado, *Philos. Trans. R. Soc. Lond. A* **368**, 1999 (2010).
7. L.E. Murr, K.N. Amato, S.J. Li, Y.X. Tian, X.Y. Cheng, S.M. Gaytan, *J. Mech. Behav. Biomed. Mater.* **4**, 1396 (2011).
8. J.M. Oblak, B.H. Kear, in *Electron Microscopy and Structure of Materials*, G. Thomas, R.M. Fulrath, R.M. Fisher, Eds. (University of California Press, Berkeley, 1972), p. 566.
9. L.E. Murr, E. Martinez, X.M. Pan, S.M. Gaytan, J.A. Castro, C.A. Terrazas, F. Medina, R.B. Wicker, D.H. Abbott, *Acta Mater.* **61** (1), 4289 (2013).
10. L.E. Murr, E. Martinez, X.M. Pan, C.M. Meng, J. Yang, S.J. Li, F. Yang, Q. Xu, J. Hernandez, W.J. Zhu, S.M. Gaytan, F. Medina, R.B. Wicker, *J. Mater. Res. Technol.* **2** (4), 376 (2013).
11. M. Orme, *J. Mater. Eng. Perform.* **2** (3), 399 (1993).
12. M. Orme, R.F. Smith, *J. Manuf. Sci. Eng.* **22** (3), 484 (2000).
13. A.A. Tseng, M.H. Lee, B. Zhao, *J. Eng. Mater. Technol.* **123** (1), 74 (2001).
14. B.U. Michaelis, D. Dunn-Rankin, R.F. Smith, J.E. Bobrow, *Int. J. Heat Mass Trans.* **50**, 4554 (2007).
15. Y.-P. Chao, L.-H. Qi, Y. Xiao, J. Luo, J.-M. Zhou, *J. Mater. Process. Technol.* **212** (2), 484 (2012). □

Where should I publish?

MRS Advances

MRS Advances reports snapshots of work in progress on key materials topics identified by MRS Meeting programming

Accepts Contributed Articles
▸ For more information visit **mrs.org/mrs-advances**

MRS Communications

MRS Communications publishes materials research that is impactful, urgent, and of broad interest to the materials community

Accepts Research Letters and Prospective Articles—forward-looking authoritative assessments of specific topics
▸ For more information visit **mrs.org/mrc**

jmr Journal of MATERIALS RESEARCH

JMR publishes materials research that demonstrates a significant scientific advance or understanding in materials science

Accepts full-length Research Articles and Reviews
▸ For more information visit **mrs.org/jmr**

MRS ENERGY & SUSTAINABILITY A Review Journal

MRS E&S addresses broad perspectives in energy and sustainability as they relate to the impact of materials research on society

Accepts Review Articles by proposal or invitation; other article formats may be considered
▸ For more information visit **mrs.org/energy-sustainability-journal**

MRS Bulletin

MRS Bulletin provides thematic materials overviews, research news, industry and policy developments, and MRS and materials community news and events

Accepts Overview Articles by invitation or proposal
▸ For more information visit **mrs.org/bulletin**

Five distinct options. One publishing partnership.

MRS Materials Research Society® | Cambridge University Press

https://doi.org/10.1557/mrs.2016.210 Published online by Cambridge University Press